Proceedings of the 2001 IEEE
International Conference on Robotics & Automation
Seoul, Korea • May 21-26, 2001

Analysis and Design Criteria for a Redundantly Actuated 4-Legged Six Degree-of-Freedom Parallel Manipulator

Byung-Ju Yi* **Daniel Cox**** **Delbert Tesar****

School of Electrical Engineering and Computer Science*
Hanyang University
Ansan, Kyungki-do, Korea

Robotics Research Group**
The University of Texas at Austin
Austin, Texas, USA

Abstract

This work introduces a new architecture for a parallel, six degree of freedom manipulator. The kinematic analysis of this redundant manipulator is provided. The proposed parallel mechanism allows easy implementation of redundant actuators, and has relatively large workspace in comparison to conventional six degree of freedom parallel devices. The kinematic analysis performed forms the basis for the introduction of design criteria for the manipulator. Several design criteria are introduced and their use is illustrated by example design involving an initial geometric parameter analysis of the manipulator.

1 Introduction

Parallel closed-chain mechanisms have been implemented often in robot design. They have some attractive advantages when compared to more commonly used serial chains. Structurally, parallel mechanisms provide alternate paths of actuation of load paths to ground. Their ability to deliver higher payload capacity, higher stiffness, etc. is compromised by a greater geometric complexity [1-12].

A greater abundance of potential input locations in structurally parallel closed-chain mechanisms allows the implementation of redundant actuation (i.e. extra input drivers). Among the many merits of redundant actuation, the ability to maintain operation under a partial system failure, or fault tolerant operation, is perhaps the most beneficial [9]. Only parallel closed-chain architectures possess the redundant actuation mode. Other capabilities include increased options for load distribution [7-11], and increased overall load capacities. Higher stiffness also leads to greater precision under load.

The Stewart Platform is perhaps the most well known parallel connection robot manipulator, which has six degrees of freedom (DOF), six legs, and six linear actuators. Stewart initially suggested using this mechanism as an aircraft simulator motion base [1]. Hunt [2], among others, suggested its use as a manipulator and addressed some alternative mechanical designs for this mechanism.

In this work, another type of six degree of freedom manipulator is investigated as shown in Figure 1. The mechanism consists of four legs, in which each leg contains an active gimbal joint, a passive revolute joint, and a passive ball joint. A special feature of this mechanism is that it can easily incorporate redundant actuation due to many potential input locations.

Additionally, the architecture of the device shown in Figure 1 allows for redundant actuation at the base of each parallel kinematic chain. This is achieved by dual redundant actuation in the active gimbal joints. Figure 2 shows the gimbal structure.

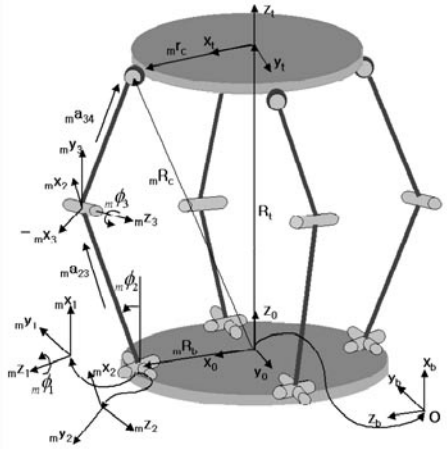

Figure 1. 4-Legged, 6-DOF Parallel Manipulator

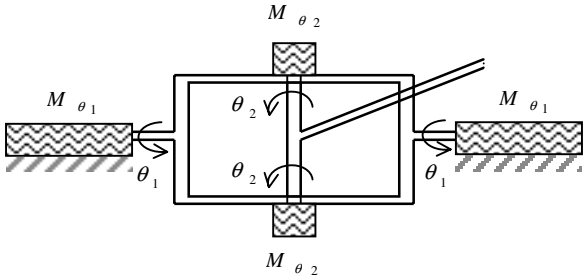

Figure 2. Gimbal Structure

Furthermore the workspace of the Stewart platform is typically small. The new mechanism has less legs than the conventional Stewart Platform, enabling the potential for more workspace and better dexterity. Thus, this paper proposes a new parallel mechanism which is not only easy to implement redundant actuators, but also has relatively large workspace in comparison to the Stewart Platform.

2 Geometric Description

The six DOF mechanism as shown in Figure 1, has four legs which connect the base plate and top plate in parallel. Each leg consists of two parallel actuated joints at the base, one passive revolute joint in the middle of the leg, and one passive ball and socket joint connecting the top, or output plate.

For simplicity of design, the four legs are distributed symmetrically. Therefore, the locations of each gimbal mechanism on the base plate are arranged in 90° increments. These displacement angles are denoted as ${}_m\gamma_{bi}$ *(i=1,...,4)* while the locations of the ball and socket joints are located similarly by ${}_m\gamma_{ti}$ on the top plate as illustrated in Figure 3.

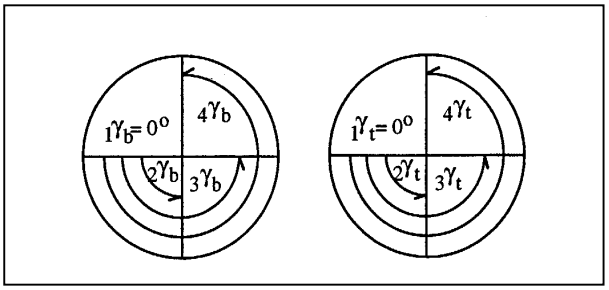

Figure 3. Displacement Angles

Two coordinate systems are defined to describe the relative position of the moving platform with respect to the base plate (see Figure 1). The coordinate system (X_0, Y_0, Z_0) fixed on the base plate is considered the global reference frame. The vector from the origin in the direction of the first gimbal joint is defined as the global X_0 axis, and the vector perpendicular to the base plate is defined as the global Z_0 axis. A moving coordinate system is attached to the moving output plate (x_t, y_t, z_t). The radii, r and R, of the top and base plates are the distances form the origin of the moving coordinate systems to the center of the ball and socket joints, and from the origin of the global coordinate system to the center of the gimbal joints, respectively. The ${}_mL_i$ *(i=1,2)* represent the lower and upper links.

3 Design Specifications and Parameters

Manipulator specifications include workspace, actuator type, payload, accuracy, weight, footprint of the manipulator, etc. In this case, consider the mechanism to be used as a force reflecting manual controller. Design specifications for this application are summarized in Table 1.

Several parameters must be considered in the design of the mechanism. Symmetry of this mechanism reduces the number of design parameters. All twist angles are set to 90°. Therefore, only four design parameters remain. These are r, R, L_1 , and L_2. The size of the gimbal mechanism should not exceed the size of R, and the maximum height of the manipulator should not exceed the limit of 30 inches to meet the requirement of manual controller [13].

Table 1. Design Specifications

Dexterous Workspace	$-45^{\circ} \le \mu_1, \mu_2 \le 45^{\circ}$ $-90^{\circ} \le \mu_3 \le 90^{\circ}$ (μ_i : Euler angles)
Payload	50 lbs.
Actuator Type	Four 2-DOF Gimbal Mechanisms with Dual DC Motors
Accuracy	0.001 in.
Weight	150 lbs. (maximum)
Footprint	10 in. diameter (maximum)
Nominal Velocity	v_0 = 40 in/s ω_0 = 6 r/s
Height	30 in. (maximum)

4 Kinematic Analysis and Design Criteria

For the design of any manipulator, a reverse position analysis is essential. The Jacobian matrix formulation is also developed to evaluate the transmission ability of the manipulator and used for design criteria [14].

4.1 Reverse Position Analysis

The position vectors ${}_m\underline{r}_c$ and ${}_m\underline{R}_b$ (see Figure 1) are the vectors from the origin of the local upper platform reference coordinate to the ball and socket joint, and from the origin of the global lower platform reference coordinate to the gimbal joint written as

$${}_1\underline{r}_c = (r,0,0)^T,\ {}_2\underline{r}_c = (0,r,0)^T,\ {}_3\underline{r}_c = (-r,0,0)^T,\ {}_4\underline{r}_c = (0,-r,0)^T. \quad (1)$$

The ${}_i\underline{R}_b$ are similar. The position vector of the ball and socket joint is denoted as

$$\begin{aligned} {}_m\underline{R}_c &= \underline{R}_t + \left[R_b^t\right]\ {}_m r_c^{(t)} \\ &= \underline{R}_t + {}_mL_1 \cdot {}_m\underline{a}_{23} + {}_mL_2 \cdot {}_m\underline{a}_{34} \end{aligned} \quad (2)$$

for *m=1,2,3,4* where the local unit vectors ${}_m\underline{a}_{23}$ and ${}_m\underline{a}_{34}$ are derived as

$${}_m\underline{a}_{23} = \begin{bmatrix} c_m\gamma_b \cdot s_m\phi_2 + s_m\gamma_b \cdot s_m\phi_1 \cdot c_m\phi_2 \\ s_m\gamma_b \cdot s_m\phi_2 - c_m\gamma_b \cdot s_m\phi_1 \cdot c_m\phi_2 \\ c_m\phi_1 \cdot c_m\phi_2 \end{bmatrix}, \quad (3)$$

and

$${}_m\underline{a}_{34} = \begin{bmatrix} c_m\gamma_b \cdot s\ {}_m\phi_{2+3} + s_m\gamma_b \cdot s_m\phi_1 \cdot c_m\phi_{2+3} \\ s_m\gamma_b \cdot s_m\phi_{2+3} - c_m\gamma_b \cdot s_m\phi_1 \cdot c_m\phi_{2+3} \\ c_m\phi_1 \cdot c_m\phi_{2+3} \end{bmatrix}, \quad (4)$$

where ${}_m\phi_{2+3} = c_m\phi_2 \cdot c_m\phi_3$. By rearranging Eq. (2)

$${}_m\underline{R}_c - {}_m\underline{R}_b = {}_mL_1 \cdot {}_m\underline{a}_{23} + {}_mL_2 \cdot {}_m\underline{a}_{34}. \quad (5)$$

Then, substitute ${}_m\underline{a}_{23}$ and ${}_m\underline{a}_{34}$ into Eq (5), the components of the vector $({}_m\underline{R}_c - {}_m\underline{R}_b)$ are

$$\begin{aligned} ({}_m\underline{R}_c - {}_m\underline{R}_b)_x &= {}_mL_1 \cdot ({}_mc_m\gamma_b \cdot s_m\phi_2 + s_m\gamma_b \cdot s_m\phi_1 \cdot c_m\phi_2) \\ &\quad + {}_mL_2 \cdot ({}_mc_m\gamma_b \cdot s\ {}_m\phi_{2+3} + s_m\gamma_b \cdot s_m\phi_1 \cdot c_m\phi_{2+3}) \end{aligned} \quad (6)$$

$$\begin{aligned} ({}_m\underline{R}_c - {}_m\underline{R}_b)_y &= {}_mL_1 \cdot (s_m\gamma_b \cdot s_m\phi_2 - c_m\gamma_b \cdot s_m\phi_1 \cdot c_m\phi_2) \\ &\quad + {}_mL_2 \cdot (s_m\gamma_b \cdot s_m\phi_{2+3} - c_m\gamma_b \cdot s_m\phi_1 \cdot c_m\phi_{2+3}) \end{aligned} \quad (7)$$

$$({}_m\underline{R}_c - {}_m\underline{R}_b)_z = ({}_mL_1 \cdot c_m\phi_2 + {}_mL_2 \cdot c_m\phi_{2+3}) \cdot c_m\phi_1. \quad (8)$$

From Eqs. (6-8), the ratio between $s_m\phi_1$ and $c_m\phi_1$ is

$$\frac{s_m\phi_1}{c_m\phi_1} = \frac{({}_m\underline{R}_c - {}_m\underline{R}_b)_x \cdot s_m\gamma_b - ({}_m\underline{R}_c - {}_m\underline{R}_b)_y \cdot c_m\gamma_b}{({}_m\underline{R}_c - {}_m\underline{R}_b)_z}. \quad (9)$$

Therefore, the first joint angle is

$${}_m\phi_1 = atan2(s_m\phi_1, c_m\phi_1). \quad (10)$$

Multiplying Eq. (6) by $s_m\phi_1$ and Eq. (7) by $c_m\phi_1$ and adding yields

$$A \cdot s_m\phi_2 + B \cdot c_m\phi_2 = C, \quad (11)$$

where

$$A = ({}_m\underline{R}_c - {}_m\underline{R}_b)_x \cdot c_m\gamma_b - ({}_m\underline{R}_c - {}_m\underline{R}_b)_y \cdot s_m\gamma_b, \quad (12)$$

$$B = \frac{({}_m\underline{R}_c - {}_m\underline{R}_b)_z}{c_m\phi_1}, \quad (13)$$

$$C = \frac{A^2 + B^2 + {}_mL_1^2 - {}_mL_2^2}{2_mL_1}. \quad (14)$$

Using the tan-half-angle laws where $t = \tan({}_m\phi_2/2)$ and substituting in Eq.(11) gives

$$t = \frac{A^2 \pm \sqrt{A^2 + B^2 - C^2}}{B + C} \quad (15)$$

to obtain

$${}_m\phi_2 = atan2(s_m\phi_2, c_m\phi_2). \quad (16)$$

Finally the third joint angle is obtained by combining Eqs. (6) and (7)

$${}_m\phi_3 = atan2({}_mL_2 \cdot s_m\phi_{2+3},\ {}_mL_2 \cdot c_m\phi_{2+3}) - {}_m\phi_2. \quad (17)$$

4.2 First-Order Analysis

The output displacement vector is defined by

$$\underline{u} = (x_t, y_t, z_t, \theta_x, \theta_y, \theta_z)^T. \quad (18)$$

The four contact points with the ball and socket joints are

$${}_m\underline{c} = ({}_1\underline{c}^T,\ {}_2\underline{c}^T,\ {}_3\underline{c}^T,\ {}_4\underline{c}^T)^T. \quad (19)$$

Each contact point vector is expressed as

$${}_m\underline{c} = \underline{R}_t + {}_m\underline{r}_{ct}. \quad (20)$$

Differentiating results in

$${}_m\dot{\underline{c}} = \dot{\underline{R}}_t + \omega \times {}_m\underline{r}_{ct}. \quad (21)$$

An alternate expression for Eq. (21) is as follows

$$ {}_m\dot{\underline{c}} = \left[{}^m G_u^c \right] \dot{\underline{u}}, \tag{22} $$

where

$$ \left[{}^m G_u^c \right] = \begin{bmatrix} 1 & 0 & 0 & 0 & {}_m r_{tz} & -{}_m r_{ty} \\ 0 & 1 & 0 & -{}_m r_{tz} & 0 & {}_m r_{tx} \\ 0 & 0 & 1 & {}_m r_{ty} & -{}_m r_{tx} & 0 \end{bmatrix}. \tag{23} $$

Then, the relationship between $\dot{\underline{c}}$ and $\dot{\underline{u}}$ is

$$ \dot{\underline{c}} = \left[G_u^c \right] \dot{\underline{u}}, \tag{24} $$

where

$$ \left[{}^m G_u^c \right] = \begin{bmatrix} \left[{}^1 G_u^c \right] \\ \left[{}^2 G_u^c \right] \\ \left[{}^3 G_u^c \right] \\ \left[{}^4 G_u^c \right] \end{bmatrix}. \tag{25} $$

The open-chain kinematics of each leg is

$$ {}_m\dot{\underline{c}} = \left[{}^m G_\phi^c \right] {}_m\dot{\underline{\phi}} \tag{26} $$

Assuming no singularities, a first-order inverse kinematics formulation is obtained as

$$ {}_m\dot{\underline{\phi}} = \left[{}_m G_c^\phi \right] {}_m\dot{\underline{c}}. \tag{27} $$

Now, the relationship between active inputs and the $\underline{c}$ coordinates is

$$ \dot{\underline{\phi}}_a = \left[G_c^a \right] \dot{\underline{c}}, \tag{28} $$

where

$$ \dot{\underline{\phi}}_a = ({}_1\dot{\phi}_1, {}_1\dot{\phi}_2, {}_2\dot{\phi}_1, {}_2\dot{\phi}_2, {}_3\dot{\phi}_1, {}_3\dot{\phi}_2, {}_4\dot{\phi}_1, {}_4\dot{\phi}_1)^T \tag{29} $$

and

$$ \left[G_c^a \right] = \begin{bmatrix} \left[{}_1 G_c^\phi \right]_{1;} & 0 & 0 & 0 \\ \left[{}_1 G_c^\phi \right]_{2;} & 0 & 0 & 0 \\ 0 & \left[{}_2 G_c^\phi \right]_{1;} & 0 & 0 \\ 0 & \left[{}_2 G_c^\phi \right]_{2;} & 0 & 0 \\ 0 & 0 & \left[{}_3 G_c^\phi \right]_{1;} & 0 \\ 0 & 0 & \left[{}_3 G_c^\phi \right]_{2;} & 0 \\ 0 & 0 & 0 & \left[{}_4 G_c^\phi \right]_{1;} \\ 0 & 0 & 0 & \left[{}_4 G_c^\phi \right]_{2;} \end{bmatrix}. \tag{30} $$

Substituting Eq. (24) into Eq. (28) yields the following

$$ \dot{\underline{\phi}}_a = \left[G_c^a \right] \dot{\underline{c}} = \left[G_u^a \right] \dot{\underline{u}}, \tag{31} $$

where

$$ \left[G_u^a \right] = \left[G_c^a \right] \left[G_u^c \right]. \tag{32} $$

The dual expression of Eq. (31) is

$$ \underline{T}_u = \left[G_u^a \right]^T \underline{T}_a, \tag{33} $$

where

$$ \underline{T}_u = \begin{bmatrix} f \\ \tau \end{bmatrix}. \tag{34} $$

4.3 Design Criteria

The operating region or workspace of a manipulator is characterized by a reachable workspace and a dexterous workspace [15]. The reachable workspace is defined as the volume or space within a reference point of the end effector which can be made to coincide with any point in space. The dexterous workspace is the volume within which the end effector has complete manipulative capability. With a reference point within the dexterous workspace, the end effector can be completely rotated about any axis through that point. A manipulator should be designed so that it has a workspace which allows its end effector to move from one regular value to another without passing through a critical value (i.e., singularity).

Several criteria have been developed to detect singular configurations particularly when considering serial structures. Structurally, parallel mechanisms consist of several open-chain structures. This type of mechanism possesses additional forms of singularities due to the interaction among the open chains. Globally, types of singularity in parallel structures can be categorized as i.) configuration dependent singularities (stationary and uncertainty configurations) ii.) algorithmic singularities, and iii.) architectural singularities. The configurations of Figures 4(b) and 4(c) are the planar views of the manipulator of Figure 4(a), illustrating respectively, the stationary and uncertainty configurations of this manipulator. Architectural singularities of the proposed manipulator can be avoided by properly locating the actuator sites.

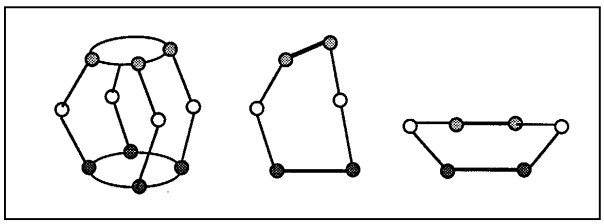

(a) (b) (c)

Figure 4. Configuration Dependent Singularities

Based on the effective force relationship of Eq. (33) between the operational force vector and the input force vector, the ratio of the 2-norm of the output load $\underline{T}_u$ to that of the input load $\underline{T}_a$ can be expressed as

$$\frac{\left\|\underline{T}_u\right\|}{\left\|\underline{T}_a\right\|} = \left[\frac{\underline{T}_a^T \left[G_u^a\right]\left[G_u^a\right]^T \underline{T}_a}{\underline{T}_a^T \underline{T}_a}\right]^{1/2} . \qquad (33)$$

Based on the Raleigh quotient [4,9], the output bounds with respect to the input loads are given as

$$\sigma_{\min}^r \left\|\underline{T}_a\right\| \le \left\|\underline{T}_u\right\| \le \sigma_{\max}^r \left\|\underline{T}_a\right\|, \qquad (34)$$

where the σ terms are the square roots of the minimum and maximum singular values of $\left[G_u^a\right]\left[G_u^a\right]^T$, respectively. Since $\left[G_u^a\right]\left[G_u^a\right]^T$ is an 8x8 matrix and has rank six, two singular values are always zero. The nonzero singular values of the 6x6 matrix $\left[G_u^a\right]^T\left[G_u^a\right]$ are the same as those of $\left[G_u^a\right]\left[G_u^a\right]^T$. The nonzero singular values are obtained in terms of $\left[G_u^a\right]^T\left[G_u^a\right]$, and these singular values are used in determining the bounds of the force transmission ratio. Note that the maximum and minimum velocity transmission ratios are defined as the inverse of the minimum and maximum force transmission ratios due to the dual nature of these concepts.

The isotropic index, or shape index is defined as the ratio of the minimum singular value to the maximum singular value of the system Jacobian and provides a measure of the shape of the transmission ellipsoid. It is given by

$$S = \frac{\sigma_{\min}}{\sigma_{\max}}, \quad 0 \le S \le 1. \qquad (35)$$

The global isotropic index (GS) is defined with respect to the entire workspace for the manipulator

$$GS = \frac{\int_W S\, dW}{\int_W dW}. \qquad (36)$$

where the integration takes place over the volume of the workspace.

The dexterous index is defined as the product of the singular values which measures the volume of the transmission ellipsoid, given as

$$D = \sigma_1 \cdot \sigma_2 \cdots \sigma_n . \qquad (37)$$

The global dexterous index (GD) is also defined with respect to the entire workspace

$$GD = \frac{\int_W D\, dW}{\int_W dW} . \qquad (38)$$

The global maximum force transmission ratio (GMFT) is defined with respect to the entire workspace of the manipulator as

$$GMFT = \frac{\int_W \sigma_{\max}^f\, dW}{\int_W dW} . \qquad (39)$$

After the above global indices are evaluated, several composite indices can be developed by combining some of the above indices. However, various design indices are usually incommensurate concepts due to differences in unit and physical meanings, and therefore should net be combined with normalization and weighting function unless they are transferred into a common domain. In other words, quantitative combination should be combined qualitatively. As the initial step to the process, preferential information should be given to each design parameter and design index. Then, each design index is transferred to a common preference design domain with ranges from zero to one. Here, the preference given to each design criterion is very subjective to the designer. Preference can be given each criterion by weighting. This provides flexibility in design. The composite design index is developed in the following.

The general design index (CDI) is formed by combining all of the design indices. For example,

a general design index which takes into account the workspace, the global isotropic index, and the global design isotropic index, and the global maximum force transmission ratio can be constructed as follows

$$CDI = \tilde{W} \wedge G\tilde{S} \wedge GM\tilde{F}T , \quad (40)$$

where " $\wedge$ " denotes the "intersection" operation [16], and $G\tilde{S}$, $\tilde{W}$ and, $GM\tilde{F}T$ given by

$$\tilde{W} = \frac{W - W_{\min}}{W_{\max} - W_{\min}}, \quad (41)$$

$$G\tilde{S} = \frac{GS - GS_{\min}}{GS_{\max} - GS_{\min}}, \quad (42)$$

$$GM\tilde{F}T = \frac{GMFT_{\max} - GMFT}{GMFT_{\max} - GMFT_{\min}} \quad (43)$$

denote a volume of the workspace, a global workspace, and a global maximum force transformation ratio, respectively, which are transferred to the same preference domain.

Note that each composition design index is constructed such that a large value represents a better design. Large $\tilde{W}$ implies that the system processes a large workspace, large $G\tilde{S}$ implies that the system possesses good isotopic characteristic within the given workspace, and large $GM\tilde{F}T$ implies that the system required small actuator effort to support a unit operational load within the given workspace. Therefore, large CDI implies that the system simultaneously possesses a large workspace, a good isotopic characteristic, and requires small actuator effort to support an unit operation load, within the given workspace.

A weighted composite design index (WCDI) can also be considered. For instance, any of the single kinematics indices, which is included in the construction of the design index, can be given more weighting compared to the others. This weighting represents the signification of the index. A weighted composite design index can be represented as follows

$$WCDI = \tilde{W}^{\alpha} \wedge G\tilde{S}^{\beta} \wedge GM\tilde{F}T^{\gamma} , \quad (44)$$

where α, β, γ represent the degrees of the weighting, and usually large values imply large weighting.

5 Initial Design Example

As an initial design, consider a mechanism of the same radii and link lengths. An optimal ratio between the link length and radius is desired in order to satisfy three criteria evenly.

The range of the two parameters (radius and link length) is from 5 inches to 14 inches. Although computationally expensive due to the inherent complexity, Figures 5(a), 5(b), and 5(c) nonetheless illustrate the plots for the global isotropic index, the global maximum force transmission ratio, and the dexterous workspace respectively. In the simulation, the entire six dimensions of the operational space are searched to obtain the global indices. Eleven points are evaluated in each direction. Specifically, it is shown that an optimal region exists with respect to the global isotropic index.

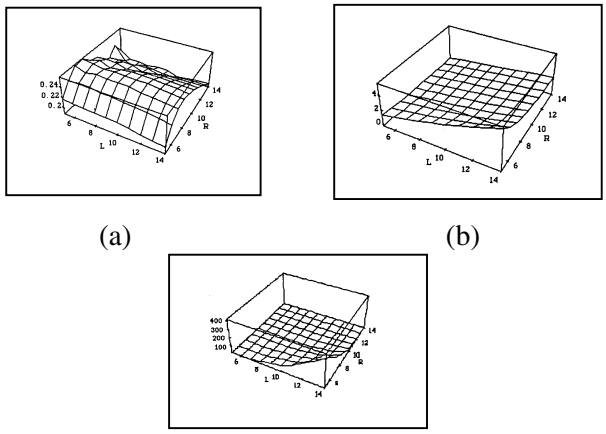

(a) (b)

(c)

Figure 5. Global Design Indices

Figures 6(a), 6(b), and 6(c) illustrate the plots for the global isotropic index, the global maximum force transmission ratio, and the dexterous workspace, which are transferred to the preference domain ranging form zero to one. Here, the best preference is given to the maximum value of dexterous workspace and the global isotropic index, and the least preference is given to the minimum value of those design criteria.

Referring to Figure 6, the best preference is given to the minimum value of the global maximum force transmission ratio, and the least preference is given to the maximum value of that design criterion. This is due to the preference for small force transmission. The designer has the flexibility in deciding the preference level for each design criterion. Now the individual composite design indices developed can be employed to obtain a set of optimal design

parameters. Figure 7 illustrates the composition design index plot which combines the three design

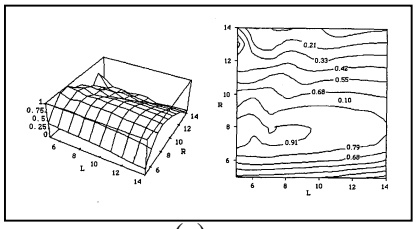

(a)

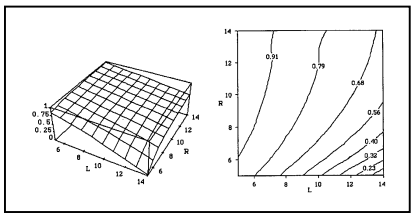

(b)

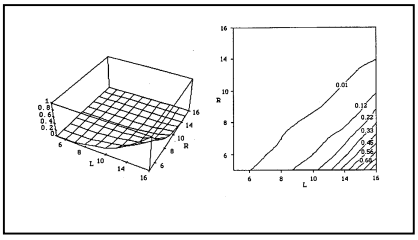

(c)

Figure 6. Global Design Indices in Preferred Domain

criteria (i.e., isotropy, force transmission, and dexterous workspace) with the same weighting. An optimal region exists along the top of the hill. Four design candidates are chosen in Table 2. Here, the dimension of the radius affects the actuator size of the gimbal mechanism. Therefore, the radius should be big enough to satisfy the platform size constraint.

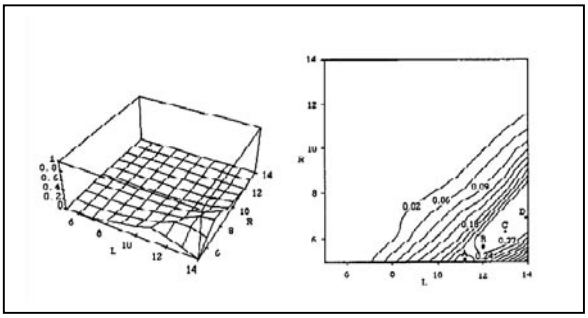

Figure 7. Composite Design Index for Initial Design

Table 2. Design Candidates for Initial Design

	A	B	C	D
L	11”	12”	13”	14”
R	5”	6”	6.5”	7”

For the Case C, the local characteristics of the manipulator are also examined in terms of the global *X* and *Z* coordinates and the rotation angle about the global *Y* axis. Figures 8(a) and 8(b) illustrate the isotropic index and maximum force transmission ratio plots in the *X-Z* plane for the initial design respectively. These plots are as follows: for each point of the *X-Z* plane, the rotation angle about the global *Y* axis is incremented from -45° to 45° and the singular values are calculated for each rotation angle. The maximum and minimum singular values are selected from this set, and the isotropic index is obtained from these values. Thus, these values are used as the contour height for the given value of the *X-Z* plane. It is shown from the isotropic index of Figure 8(a) that a good isotropic region is located in the upper part of the workspace. The global maximum force transmission characteristic, as shown in Figure 8(b) is shown to have even distribution throughout the entire workspace. The flat regions of these plots denote out-of-bound workspace for the mechanism. The workspace of the proposed manipulator is much larger than that of Stewart platform type manipulator for the same system size. This is due to employment of revolute joint in the knuckle.

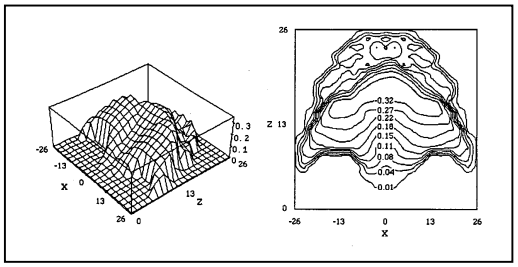

(a)

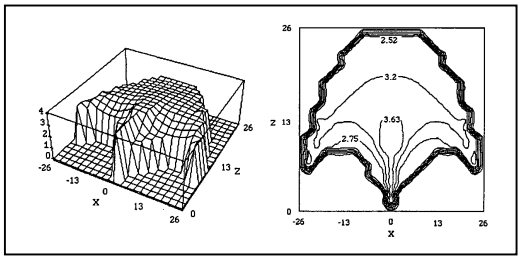

(b)

Figure 8. Local Analysis of *X-Z* Plane for the Initial Design

Another report [10] related to redundant actuation shows that doubling the number of actuators increases the payload more than four times. Based on this information, for the redundantly actuated parallel mechanism proposed in this work, employing two more actuators resulting from adding up one more leg will increase the payload more than 270% [14]. Thus, the main contribution of this report can be summarized as follows. The proposed parallel mechanism allows easy implementation of redundant actuators with improvement in payload, and has relatively large workspace in comparison to conventional six degree of freedom parallel devices.

6 Conclusion and Future Work

A new six DOF parallel manipulator is investigated in this work. The kinematic analysis for the device is presented including discussion of singularity configurations. Single design indices used as design criteria are introduced. An initial example design demonstrates the use of these design criteria. Future work in combining the individual design criteria into multi-criteria composite design indices for optimal design of the mechanism presented in this paper is being pursued. This will enable a more powerful dimensional synthesis for the design parameters in order to explore and compare alternative designs. Future collaborations also include investigation of fault tolerant redundant actuation strategies using the four-legged, six degree of freedom manipulator.

References

[1] Stewart, D., " 1965, "A platform with 6 Degrees of freedom," Proc. Of Institution of Mechanical Engineers, 1965-1966, Part 1, No. 15, pp. 371-386.

[2] Hunt, K.H., 1983, "Structural kinematics of in-parallel-actuated robot arms," ASME Trans. Journal of Mechanisms, Transmissions, Automation in Design, Vol. 105, pp. 705-712.

[3] Freeman, R.A. and Tesar, D., 1988, "Dynamic modeling of serial and parallel mechanisms/linkage systems, Part I-Methodology, Part II-Applications," 20th Biennial Mechanism Conf., Kissimmee, FL. DE-Vol. 15-2, pp. 7-21.

[4] Kim, W.K., 1989, "Architectural study of the design and operation of advanced force feedback manual controllers," Ph.D. Dissertation of Mechanical Engineering, The University of Texas at Austin.

[5] Ma, O. and Angeles, J., 1991, "Architectural singularities of platform manipulators," Proc. IEEE Int. Conf. On Robotics and Automation, Sacramento, CA. pp. 1542-1547.

[6] Kim, D.I., Chung, W.K., 1999, "Analytic Singularity equation and Analysis of 6-DOF Parallel manipulators Using Local Structurization Method," IEEE Trans. Robotics and Automation, Vol.15, No.4, pp.612-622.

[7] Kumar, V.J. and Gardner, J., 1990, "Kinematics of redundantly actuated closed chains," IEEE Trans. on Robotics and Automation, Vol.6, No.2, pp.269-273.

[8] Kurz, R. and Hayward, W., 1990, "Multiple goal kinematic optimization of a parallel spherical mechanism with actuator redundancy," IEEE Trans. on Robotics and Automation, Vol. 8, No. 5, pp. 644-651.

[9] Yi, B.J., Freeman, R.A., and Tesar, D., 1990, "Analysis of a redundantly actuated fault–tolerant spherical shoulder module," Proc. of Biennial Mechanism Conf. at Orlando, FL.

[10] Yi,B.J.,Oh, S.R., Suh, I.H., 1999 "A five-bar finger mechanism involving redundant actuator : Analysis and its application," IEEE Trans. on Robotics and Automation, Vol.15, No.6, pp.1001-1010.

[11] Cox D., and Tesar, D., 1989 "The dynamic model of a three degree of freedom parallel robotic shoulder module," Proc. of Fourth International Conference on Advanced Robotics, Springer-Verlag, pp. 475-487.

[12] Ji, P., and Wu, H.T., 2000, "A fast solution to identify placement parameters for modular platform manipulators," Journal of Robotic Systems, Vol. 17, No. 5, pp. 251-253.

[13] Parsons. H.M., 1985, "Human factors engineering issues in army field robotics applications," Prepared for the U.S. Army Human Engineering Laboratory, Aberdeen Proving Ground, MD. Hunsville, Essex Corp.

[14] Yi, B.J. and Tesar, D., 1992, "On the optimal design of a redundantly actuated 4-legged six degree of freedom manipulator," Internal report, The University of Texas at Austin.

[15] Kumar, V.J., and Waldron, K.J., 1981, "The workspace of a mechanical manipulator," ASME Journal of Mechanical Design, Vol. 103, pp.665-672.

[16] Terano, et.al., Asai, K., and Sugeno, M., 1992, "Fuzzy systems theory and its applications," Academic press, INC., Harcourt Brace Jovanovich, Publishers.